Dewetting of PtCu Nanoalloys on TiO_2 Nanocavities Provides a Synergistic Photocatalytic Enhancement for Efficient H_2 Evolution

Fahimeh Shahvaranfard,[a] Paolo Ghigna,[b] Alessandro Minguzzi,[c]

Ewa Wierzbicka,[a] Patrik Schmuki,[a,d]* Marco Altomare[a]*

[a] Institute for Surface Science and Corrosion WW4-LKO, Department of Materials Science and Engineering, University of Erlangen-Nuremberg, Martensstrasse 7, 91058 Erlangen, Germany

[b] Dipartimento di Chimica, Università degli Studi di Pavia, Viale Taramelli 13, 27100 Pavia, Italy

[c] Dipartimento di Chimica, Università degli Studi di Milano, Via Golgi 19, 20133 Milan, Italy

[d] Chemistry Department, Faculty of Sciences, King Abdulaziz University, 80203 Jeddah, Kingdom of Saudi Arabia

* Corresponding Author. E-mail: schmuki@ww.uni-erlangen.de

marco.altomare@fau.de

A B S T R A C T

We investigate the co-catalytic activity of PtCu alloy nanoparticles for photocatalytic H_2 evolution from methanol-water solutions. To produce the photocatalysts, a few nm-thick Pt-Cu bilayers are deposited on anodic TiO_2 nanocavity arrays and converted by solid state dewetting, i.e. a suitable thermal treatment, into bimetallic PtCu nanoparticles. XRD and XPS results prove the formation of PtCu nanoalloys that carry a shell of surface oxides. XANES data support Pt and Cu alloying and indicate the presence of lattice disorder in the PtCu nanoparticles. The PtCu co-catalyst on TiO_2 shows a synergistic activity enhancement and a significantly higher activity towards photocatalytic H_2 evolution than Pt- or Cu-TiO_2. We propose the enhanced activity to be due to Pt-Cu electronic interactions, where Cu increases the electron density on Pt favoring a more efficient electron transfer for H_2 evolution. In addition, Cu can further promote the photo-activity by providing additional surface catalytic sites for hydrogen recombination. Remarkably, when increasing the methanol concentration up to 50 vol% in the reaction phase, we observe for PtCu-TiO_2 a steeper activity increase compared to Pt-TiO_2. A further increase in methanol concentration (up to 80 vol%) causes for Pt-TiO_2 a clear activity decay, while PtCu-TiO_2 still maintains a high level of activity. This suggests an improved robustness of PtCu nanoalloys against poisoning from methanol oxidation products such as CO.

Keywords: TiO_2 nanotube, solid-state dewetting, platinum, copper, PtCu alloy nanoparticle, photocatalysis, H_2 evolution

1. Introduction

The generation of hydrogen from water on an illuminated semiconductor has been pioneered by Fujishima and Honda in 1972.[1] Ever since then, titanium dioxide (TiO_2) has been envisaged as a most promising photocatalytic material for H_2 evolution due to some key features, i.e. a suitable conduction band (CB) edge with respect to the redox potential of H_2O to H_2, its low cost, its large availability and its high chemical and photochemical stability.[2–4]

TiO_2, as an oxide sub-stoichiometric semiconductor, suffers however from intrinsic limits such as a fast recombination of photogenerated charge carriers, and a sluggish kinetic of charge transfer to reactants at the semiconductor/environment interface. This causes a poor photocatalytic performance.[5,6] One-dimensional (1D) TiO_2 nanostructures, such as nanotubes, nanorods or nanowires, can provide a short diffusion distance and a directional pathway for photogenerated charge carriers, hence limiting charge recombination and improving the photo-activity.[7,8]

Except for nanostructuring, another strategy to enhance the photocatalytic performance is to deposit on the TiO_2 surface a suitable co-catalyst. Co-catalysts that can promote the H_2 evolution reaction are noble metal nanoparticle (NPs) e.g. Pt, Au or Pd. Pt, due to its higher work function (i.e. it forms a higher metal/semiconductor Schottky barrier), can efficiently trap photogenerated TiO_2 CB electrons and mediated their transfer to the environment. Pt offers also suitable catalytic surface sites for hydrogen recombination.[9,10] Its low abundance has however pushed the research towards the identification of earth abundant, cost-effective co-catalysts.

Metals such as Ni, Cu or Co, are largely available but their individual activity is comparably poor. Nonetheless, their combination with noble metals in the form of bimetallic (or multimetallic) systems can lead to significantly higher activities than those showed by the monometallic constituents.[11–14] The catalytic improvement, in general, is associated to the atomic structure of the

alloy catalyst and can be ascribed to electronic, geometric, or synergistic effects.[12] Bimetallic catalysts can also block undesired reaction paths or prevent poisoning from by-products.[15,16]

In this context, PtCu alloys have attracted large attention as they can provide a remarkable activity enhancement compared to Pt alone in different catalytic processes such as oxygen reduction,[17] CO_2 conversion,[18] or NO reduction.[19] Here alloying allows also to minimize the amount of Pt used. In addition, bimetallic PtCu nanoparticles or PtCu alloys demonstrated a superior catalytic activity and tolerance for the electrochemical oxidation of light molecules, such as methanol or formic acid.[12,20–22]

Combinations of noble metals (e.g. Pt or Au) and Cu catalysts have been explored also in photocatalysis. TiO_2 powders modified with grafted Cu species and Pt NPs showed promising photocatalytic H_2 evolution performances. This was explained in terms of a reversible switch of the Cu oxidation state ($Cu^{2+} \leftrightarrow Cu^{+}$) that favors an efficient electron transfer via Pt to protons for H_2 evolution.[23] Other studies on PtCu-TiO_2[24] or Au-Cu_2O-TiO_2[25] photocatalysts propose a reduction of oxidized Cu species to Cu metal during the early stage of illumination leading to bimetallic (PtCu or AuCu) systems where Cu promotes the photocatalytic performance by increasing the electron density on Pt and by providing catalytic surface sites for hydrogen recombination.

PtCu NPs can be produced by different methods including photo-deposition,[26] galvanic replacement,[12] impregnation,[27] chemical reduction[28] or colloidal chemistry.[29] In a recent work[30] we reported on a straightforward "sputtering-dewetting-alloying" approach to produce bimetallic (e.g. NiCu) nanoparticles directly on photocatalytic TiO_2 surfaces.

Herein, we use such a dewetting-alloying concept to produce a TiO_2 photocatalyst for H_2 evolution co-catalyzed by bimetallic PtCu nanoparticles. For this, we sequentially coat TiO_2 NT arrays with

few nm thick Pt and Cu films. Then, we trigger dewetting of the Pt-Cu bilayers by a suitable heat treatment,[31] that is, the Pt and Cu films break up, agglomerate and intermix, forming dewetted-alloyed PtCu NPs at the NT surface. We vary the Pt and Cu content in the NPs by adjusting the initial thicknesses of the Pt and Cu films, i.e. by tuning the bilayer initial composition.

Our results show that PtCu NPs of an optimized composition can lead to a remarkable synergistic enhancement in photocatalytic hydrogen evolution compared to Pt or Cu monometallic co-catalysts due to an improved charge transfer efficiency to adsorbed H^+. Moreover, our results indicate that the presence of Cu in the bimetallic co-catalyst promotes an enhanced performance even for high concentration of methanol (used as hole-scavenger) in the reaction phase, while Pt-TiO_2 under such reaction conditions is subject to a substantial loss of activity. This suggests either that the bimetallic PtCu co-catalyst promotes the complete oxidation of methanol to CO_2 (hence minimizing the formation of CO that can poison Pt active sites) or that Cu improves the resistance of the co-catalyst to poisoning, likely by weakening the binding strength of methanol oxidation intermediates (CO) to Pt sites. This results in a photocatalyst for photo-reforming of organic-water mixtures that allows to generate H_2 at a higher rate than Pt-TiO_2 systems and well tolerates high organic concentrations in the reaction phase.

2. Experimental Section

2.1. Growth of TiO_2 nanotube arrays

Key to a high degree of self-ordering for anodic TiO_2 nanotube arrays is to establish electrochemical conditions that during anodization lead to high rate of oxide growth combined to a high rate of oxide dissolution.[32–34] This can be achieved by anodizing Ti metal in hot o-H_3PO_4/HF electrolytes.[34,35] The growth conditions can be adjusted to form a short tube length that resembles

a nanocavity. The resulting arrays of TiO_2 nanotubes can be formed over large surfaces, even up to some 10 cm^2,[36] and present a virtually ideal hexagonal packing.

In the present work, to grow such nanotube arrays, Ti foils (30×15 mm^2, 0.125 mm thick, Advent Research Materials, 99.6+% purity) were cleaned by ultrasonication in acetone, ethanol and DI water, and then dried with nitrogen. Anodization was carried out in an electrolyte consisting of 3 M HF in o-H_3PO_4 (Sigma- Aldrich) at 105°C, by applying a potential of 15 V for 2 h. After anodization, the samples were rinsed with ethanol, soaked in ethanol overnight and then dried with nitrogen.

2.2. Metal film deposition and solid state dewetting

In order to form Pt, Cu and alloyed PtCu nanoparticle on the TiO_2 nanotube arrays, an Ar-plasma sputtering machine (EM SCD500, Leica) was used to deposit thin metal films, followed by a solid state dewetting step.

Metal (Pt or Cu) films, or metal bilayers (Pt-Cu) of different thicknesses were deposited on the anodic TiO_2 nanotube structures. As metal targets we used a 99.99% pure Pt target (Hauner Metallische Werkstoffe) and a 99.90% pure Cu target (Baltic Praeparation e.K.). The sputtering was performed at an applied current of 16 mA and at a chamber pressure of 10^{-2} mbar of Ar.

A solid state dewetting[31] approach was then used to convert the thin metal films into dispersions of defined metal particles at the nanostructured oxide surface. The overall driving force for dewetting is the minimization of the free surface energy of the metal film, of the substrate and of the metal-substrate interface. Given that the thinner the metal film the higher its surface-to-volume ratio and thus its surface energy, the driving force for dewetting increases dramatically when the film thickness decreases. In other words, the thinner the metal film the lower the activation energy

for metal atom surface mobility. This is the key reason why dewetting can be triggered at temperatures that are well below the film melting point, i.e. the film dewets while remaining in the solid state.[31,36]

In the present work, after metal film sputtering, the samples were annealed at 500°C, for 1 h in Argon atmosphere (Ar flux = 10 L h^{-1}), to induce solid state dewetting of the metal films and form directly at the NT surface Pt, Cu or bimetallic PtCu nanoparticles.

Samples are named according to the co-catalyst nature and composition, depending on the initial thickness of the dewetted metal film(s): e.g. "Pt*x*Cu*y*-TiO_2", where "*x*" and "*y*" are the nominal thicknesses of the sputtered metal films expressed in nm. TiO_2 samples loaded with monometallic (Pt or Cu) NPs are labelled as "Pt*x*-TiO_2" or "Cu*y*-TiO_2".

2.3. Characterization of the structures

A field-emission scanning electron microscope (FE-SEM, Hitachi S4800) was used to study the morphology of the samples. The crystallographic properties of the samples were examined by X-ray diffraction (XRD) with an X′pert Philips MPD (equipped with a Panalytical X'celerator detector). X-ray photoelectron spectroscopy (XPS, PHI 5600, US) was employed to analyze the chemical composition of the samples. Diffusive reflectance spectra of the different samples were measured by a fiber-based UV-vis-IR spectrophotometer (Avantes, ULS2048) equipped with an integrating sphere AvaSphere-30 using an AvaLight-DH-S-BAL balanced power light source.

X-ray absorption spectroscopy (XAS) at the Pt L_{III}-edge (11564 eV) and Cu K-edge (8979 eV) was carried out in the fluorescence mode at the P65 beamline of the Petra III synchrotron radiation facility (Hamburg, Germany), using a Si(311) double crystal monochromator, and a passivated implanted planar silicon (PIPS) detector, allowing for collecting a full extended X-ray absorption

fine structure (EXAFS) spectrum in ca. 15-20 min. The energy calibration was performed by measuring the absorption spectrum of a metallic Cu foil at the Cu-K edge. The spectra of the reference samples (metallic Cu and Pt, CuO and Cu_2O) were acquired in the transmission mode. For these measurements, a proper amount of sample, as to give a unit increase in the absorption coefficient, was mixed with cellulose and pressed into a pellet. All data were obtained at room temperature. The X-ray signal extraction and normalization was performed by means of the ATHENA code, belonging to the set of interactive programs IFEFFIT.[37] The pre-edge back ground was fitted by means of a straight line and the post edge background by means of a cubic spline. The EXAFS data analysis was performed with the EXCURVE code using a k^2 weighing scheme.

2.4. Photocatalytic experiments

Photocatalytic measurements for H_2 generation were conducted by irradiating the metal NP decorated oxide films in water, methanol, methanol-water (with different MeOH contents) or ethanol-water (20% EtOH) mixtures in a quartz tube sealed up with a rubber septum. As irradiation source a UV LED (Opsytec, Germany λ = 365 nm, beam size = 0.785 cm^2, power of ~ 100 mW cm^{-2}) was used. H_2 evolution experiments were carried out for the most active sample (Pt2.5Cu2.5) also under irradiation provided by a filtered (420 nm cutoff filter) AM 1.5 G simulated solar light (100 mW cm^{-2}, Solarlight, USA, 300 W Xe lamp with Solar light optical filter) and by a monochromatic 450 nm laser (2 W, OdicForce Lasers).

Prior to photocatalysis, to remove oxygen, the cell was purged with Ar gas for 20 min. The amount of accumulated H_2 in the head space of the quartz tube during irradiation was determined by means of gas chromatography (GC-MSQO2010SE, Shimadzu, Japan). The GC was equipped with a thermal conductivity detector (TCD), a Restek micro packed Shin Carbon ST column (2 m

x 0.53 mm) and a Zebron capillary column ZB05 MS (30 m x 0.25 mm). GC measurements were conducted at oven temperature, 45°C (isothermal conditions), with the temperature of the injector set at 280°C and that of the TCD fixed at 260°C. The carrier gas (argon) flow rate was 14.3 mL min^{-1}.

3. Result and Discussion

Fig. 1a shows SEM images of highly ordered TiO_2 nanotubes ("nanocavities") grown by anodization of Ti foil in a hot HF/o-H_3PO_4 electrolyte.[38] Additional SEM images are provided in Fig. S1. These nanostructures show an ideal hexagonal packing (top view) and have an average length of ~ 200 nm and inner diameter of ~ 100 nm (cross sectional view – inset in Fig. 1a). Such semiconductor geometry is ideal for the subsequent metal film deposition-dewetting step.

Fig. 1b-f show the result of metal sputter-coating of Pt (5 nm) and Cu (5 nm) films or Pt-Cu bilayers on TiO_2 NTs followed by dewetting at 500°C in Ar. As shown in Figure S2, the TiO_2 NTs were homogenously covered by the sputtered metal (nominal film thickness 5 nm), regardless of the film composition (Pt, Cu or Pt-Cu). One can see from Figure 1b-f that the thermal treatment causes the conversion via surface diffusion of all metal films and bilayers into metal nanoparticles. It is reported that dewetting generally initiates at temperatures between 1/3 and 1/2 of the metal melting point.[31] The occurrence of dewetting of Cu at 500°C is well in line with its melting points (T_m = 1085°C).[37] Dewetting of Pt films (and Pt-Cu bilayers) would in principle be expected to take place at higher temperatures, given the melting point of Pt of 1768°C. Nevertheless the films studied in the present work are rather thin (nominal thickness ≤ 5 nm), and can hence dewet at lower temperatures as, in general, the thinner the film the lower the T_{dewet}.[31]

The dewetted nanoparticles show a similar average size (Fig. S3). The Pt film and the different Pt-Cu bilayers dewet into particles with a mean size in the 5-15 nm range. Minor differences are

observed for the pure Cu NPs, the size of which is in average slightly larger, i.e. 5-20 nm. A similar trend was observed also in previous work[30] and can be explained taking into account the lower melting point and higher surface mobility of Cu.

A series of TiO_2 NT arrays decorated with dewetted Pt, Cu or PtCu NPs (prepared by systematically varying the nominal thickness of the Pt and Cu films) were characterized by XRD in view of their crystallographic features.

The XRD results are shown in Fig. 2. All patterns (Fig. 2a) feature dominant diffraction signals at 38.4° and 40.1° ascribed to the 002 and 101 reflections of metallic Ti. Such signals originates from the Ti metal substrate. Anodic TiO_2 NT layers, as reported in the literature, are typically amorphous in the as-grown state.[2] The thermal treatment at 500°C in argon leads to the crystallization of the NT layers into a mixed anatase-rutile TiO_2 phase, as proved by the peaks at 25.3° and 27.5° that can be ascribed to the anatase 101 and rutile 110 reflections, respectively. The crystallization of the NTs forms also minor amounts of a Ti oxyfluoride phase, giving rise to the peak at 22.8° that can be attributed to the 200 reflection of $TiOF_2$. Such a compound may originate from a solid-state reaction (during the thermal treatment) between the oxide and fluoride species up-taken from the anodizing electrolyte during the NT growth. Besides, the content of anatase phase is in general higher than that of rutile for most samples, though a different anatase-rutile relative composition was observed for NTs decorated with pure Cu NPs (sample Cu5). In this case, the presence of Cu alone seems to favor the crystallization of the NTs into rutile phase (as observed also in previous work[30,37]).

Fig. 2b shows an enlarged view in the 45-52° 2θ region of the patterns shown in Fig. 2a. The XRD pattern of sample Pt5 shows signals at 39.7°, 46.4° and 67.8° that correspond to the Pt 111, 200 and 220 diffraction peaks, confirming the metallic nature of the dewetted Pt NPs. The XRD

pattern of sample Cu5 shows signals at 43.3°, 50.5° and 74.0° that can be attributed to the 111, 200 and 220 crystallographic planes of Cu metal, respectively.[11,39]

Interestingly, samples produced by dewetting Pt-Cu bilayers show a shift of the signals of Pt towards larger angles and of Cu towards smaller angles. I.e. for sample Pt2.5Cu2.5, no Pt 200 peak is found at 46.4° and no Cu 200 reflection appears at 50.5°. Instead, only one signal can be seen at 48.1° that can be assigned to the 200 reflection of a bimetallic PtCu phase. This confirms the occurrence of Pt and Cu alloying during dewetting (in line with what is also reported for other dewetted metal combinations[37,40]), i.e. the bilayer, when treated at 500°C in Ar, breaks up and agglomerates causing Pt and Cu to intermix forming dewetted-alloyed PtCu NPs at the TiO_2 NT surface. The position of the 200 peak is well in line with the Vegard's law,[30,41] that is, the lattice constant of the PtCu phase correlates with a linear combination of the 200 peak positions of pure Pt and Cu phases and of their molar fraction in the binary PtCu system. In addition, the XRD peaks of the dewetted NPs are broad and relatively weak, which suggest a low degree of crystallinity or structural disorder in the bimetallic NPs (see the discussion of XAS data below).

To further study the physicochemical differences between mono- and bimetallic co-catalysts, samples Pt2.5, Pt2.5Cu2.5 and Cu2.5 were characterized by XPS and XAS.

XPS surveys for these samples are shown in Fig. S4 while their surface composition data are compiled in Table S1. In general, the data show the structures to be composed of Ti, O, adventitious C, and Pt and/or Cu in line with the composition of the sputtered-dewetted metal films.

High resolution XPS spectra are shown in Fig. 3a-b while Fig. 3c shows Cu and Pt speciation determined by fitting the HR XPS spectra. Fig.3a provides the Pt 4f XPS spectra for the samples Pt2.5 and Pt2.5Cu2.5. The fit of the spectrum of sample Pt2.5 shows signals at 70.7 and 74.0 eV

that can be attributed to the Pt $4f_{7/2}$ and Pt $4f_{5/2}$ signals of metallic Pt. The small peaks at 71.9 and 75.4 eV can account for minor contents (~ 10 at%) of Pt(II) species, likely Pt(II) oxides (see quantitative data in Fig. 3c).[42] Similar spectra were obtained for the sample decorated with the bimetallic co-catalyst, i.e. Pt2.5Cu2.5. Here, however, one can notice a positive shift of 0.3 eV in the binding energy values of the Pt $4f_{7/2}$ and Pt $4f_{5/2}$ peaks. This proves an intimate interaction of Pt and Cu in the dewetted bimetallic nanoparticles and hence corroborate the XRD results supporting the formation of PtCu nanoalloys.[26,42,43] Besides, small peaks at 72.2 and 75.7 eV are also observed for sample Pt2.5Cu2.5 which can account for comparable contents of Pt(II) oxides. It should be mentioned that the presence of Pt(II) oxides (as well as Pt(IV) species) on dewetted Pt nanoparticles has been reported also in previous work.[44]

Fig. 3b shows the Cu 2p spectra for samples Cu2.5 and Pt2.5Cu2.5. The Cu 2p spectrum of sample Cu2.5 clearly shows the coexistence of different oxidation states of copper, such as metallic Cu with the characteristic Cu $2p_{3/2}$ and Cu $2p_{1/2}$ doublet located at 932.4 and 952.2 eV, and Cu(II) (likely CuO) the signal of which can be fitted with two peaks at 934.4 (Cu $2p_{3/2}$) and 954.4 eV (Cu $2p_{1/2}$). Cu(II) species also show the characteristic satellite features at ca. 940 and 962 eV,[45] and hence one can conclude that Cu(I) species are either not present at surface of the NPs or that their content is minor. The Cu 2p spectrum of sample Pt2.5Cu2.5 shows a shift of 0.3 eV to lower binding energy (i.e. a negative B.E. shift) with respect to that of pure Cu NPs (sample Cu2.5) – this provides a first evidence that Cu and Pt are in intimate contact in dewetted-alloyed PtCu NPs.

Based on such results, one may suggest that the dewetted NPs feature a metallic core carrying an oxide shell. The latter forms likely after dewetting, when the samples are exposed to oxygen under ambient conditions. This explains for example the particularly high O surface content measured by XPS for sample Cu2.5 (see data in Fig. 3c).

We also characterized samples Pt5-TiO_2 and Cu5-TiO_2 by XPS. The results are shown in Fig. S5a,b, along with the samples' composition in terms of relative metal vs. oxide content obtained from XPS fitting (Fig. S5c). These data should be compared to results for Pt2.5-, Cu2.5- and Pt2.5Cu2.5 systems in Fig. 3. Comparing the quantitative data for Pt-, Cu-, and PtCu-systems shows that the relative metal vs. oxide content in the dewetted nanoparticles does not change significantly with the particle size.

Interestingly, the Cu 2p XPS spectrum of sample Pt2.5Cu2.5 (Fig. 3b) shows that the co-catalyst NPs contain Cu mainly in the metallic state, in line with the dominant Cu $2p_{3/2}$ and Cu $2p_{1/2}$ doublet located at 932.1 and 951.9 eV, while the signal of Cu(II) species is negligible (see for comparison the quantitative data in Fig. 3c). This supports once more the interaction in the bimetallic NPs between Cu and Pt, where in this case the presence of Pt seems to prevent Cu from oxidation under ambient conditions. It should be noted that the Gibbs free energy of dissolution of metallic Cu in Pt is negative at any mixing ratio.[46] The formation of a Pt-Cu alloy therefore gives a stabilizing contribution term for Cu(0) – this may be the origin of the protection effect against Cu oxidation observed for the PtCu NPs.

In principle, based on plain electronegativity effects, the XPS shift occurring with alloying is expected for Pt to be negative (shift towards lower B.E. values) while it should be positive for Cu (shift towards higher B.E. values). Our results, though apparently in contradiction with the expected shifts, are nonetheless in line with what reported in various previous studies on PtCu nanoalloys.[26,42,47,48] This suggests that not only the alloy composition but likely also electronic or structural effects, or the presence of additional compounds (oxides, as in our case), may affect the Pt and Cu B.E. values and the resulting shifts observed.

We found various reports where for bimetallic systems the XPS signals showed anomalies in the binding energy shift.[26,42,47–49] Such anomalies have been explained e.g. by a charge compensation model as reported by Watson et al.[49] In the case of Pt-Cu systems, positive ("anomalous") shifts for the Pt signal have been observed in the literature in a number of reports,[26,42,48] and particularly relevant are the findings reported for Pt-Co alloys.[47] It has been proposed that: when Pt atoms are alloyed with a second component the total number of electrons per Pt atom increases, while the number of 5d electrons decreases, accompanied by a re-hybridization of the d-band as well as of the sp-band, which leads to an upshift of the reference level (Fermi energy), resulting in an opposite downshift of Pt 4f7/2 level. Such electronic effects were shown to cause, as a net effect, a positive B.E. shift for Pt when alloyed with metals such as Co or Cu.

XANES spectra for samples Pt5, Pt2.5Cu2.5 and Cu5, as well as for reference materials (Pt and Cu foils, and Cu_2O and CuO pellets) are shown in Fig. 4a,b. At the Pt L_3-edge, the edge energy position and shape show that Pt is present in the metallic state. The structure at ca. 11580 eV is broadened in the sample Pt5 with respect to the Pt foil reference, and even more broadening is apparent in the spectrum of the sample Pt2.5Cu2.5. In general, broadening of features in XAS spectra is indicative of the presence of disorder; for example, Lytle et al.[50] attributed the broader structure of the Pt L_3 edge in Pt catalysts (compared to a reference metal foil) to nano-size effects in the former. We can therefore conclude that Pt in the dewetted NPs is more disordered than the metallic Pt reference (foil), and the disorder is in sample Pt2.5Cu2.5 even more pronounced with respect to sample Pt5 due to alloying effects. The increased disorder is in agreement with the diffraction patterns shown in Fig. 2 (peak broadening). The EXAFS spectra at the Pt L_3-edge of the two samples were fitted using a Pt metal model. The fits are shown in the Fig. 4c-f. The fitting results are given in Table S2 (n: coordination number, r: coordination distance, r_0: crystallographic

distance in metallic Pt, σ^2: EXAFS Debye-Waller factor). The nearest neighbor distance in sample Pt2.5Cu2.5 sample is lower than in sample Pt5. This likely indicates that in sample Pt2.5Cu2.5, Cu is incorporated in the Pt lattice (atomic radii: Pt 1.75 Å, Cu 1.40 Å).

The XANES data at the Cu K-edge are shown in the Fig. 4b, along with spectra of standard compounds for the different oxidation states of Cu. The spectrum of sample Pt2.5Cu2.5 shows the presence of mostly Cu(II) with some amounts of Cu(I), while the spectrum of sample Cu5 shows the presence of both Cu(I) and Cu(II) in comparable amounts. It should be noted, however, that a precise quantification of the amounts of Cu in the different oxidation states is made difficult by the lack of an evident edge structure. Using the same argument as above, this can be attributed to the presence of disorder in the dewetted NPs, in agreement with their nanostructured nature as evidenced by XRD. This disorder prevents further analysis of these spectra. However, XANES results at the Cu K-edge agree well with XPS data, once the sensibility of XPS to near surface information is taken into account.

The different samples were then studied as photocatalysts for H_2 evolution from methanol-water mixtures under UV light illumination. Methanol was selected as a hole scavenger (e.g. instead of ethanol) as in preliminary experiments the former allowed to reach higher H_2 evolution rates (Fig. S7), as also found in previous work. More details can be found in the supporting information.

Fig. 5a shows the photocatalytic activity of pristine TiO_2 NTs along with that of NT layers decorated with dewetted Pt, Cu or PtCu NPs. The data indicate that, as expected, pristine TiO_2 NTs show a negligible H_2 generation rate (0.06 μL h^{-1} cm^{-2}) while structures decorated with Pt NPs (sample Pt5) evolve H_2 at a higher rate, i.e. 12.9 μL h^{-1} cm^{-2}. The activity of NTs modified with dewetted Cu NPs is 1.0 μL h^{-1} cm^{-2}, i.e. clearly lower than that of Pt-TiO_2 systems and in line with previous work.[30] As widely reported in the literature,[51–53] the presence of Pt NPs on the

TiO_2 surface is beneficial to the photoactivity due to the high work function of Pt (5.1-5.9 eV) with respect to the Fermi level of TiO_2 (4.6-4.7 eV). This results in the formation of a relatively high Schottky barrier that allows for efficient trapping of TiO_2 CB electrons in the Pt NPs and their transfer to H^+ for H_2 evolution. The lower work function of Cu (4.5-5.1 eV) explains the comparably poor activity of Cu-TiO_2 systems, i.e. the height of the formed Schottky barrier is comparably small leading to a less efficient electron trap.

Most importantly, dewetted bimetallic NPs with equal nominal loadings of Pt and Cu (sample Pt2.5Cu2.5) co-catalyze TiO_2 NTs for H_2 generation with the highest efficiency, leading to H_2 evolution rates as high as 50.7 μL h^{-1} cm^{-2}, which is ~4 and ~50 times higher than the activity of NTs modified with pure Pt (sample Pt5) and pure Cu (Cu5) NPs, respectively. The nominal relative Pt:Cu content for sample Pt2.5Cu2.5 is 0.70:0.30 wt% or 0.44:0.56 at%. Similar activity enhancements for Pt and Cu co-modified photocatalysts are reported also in previous reports but smaller relative amounts of Cu (≤ 0.1 wt%), i.e. higher Pt relative contents, were shown to enable a clear performance enhancement.[23]

The activity enhancement we observe is remarkable and is far larger than simple additive effects, i.e. is synergistic as the sum of the activity of pure Pt and Cu co-catalyst NPs yields a H_2 evolution rate of ~ 14.0 μL h^{-1} cm^{-2}, which is substantially lower than the rate of 50.7 μL h^{-1} cm^{-2} delivered by the bimetallic co-catalyst.

The co-catalytic activity of other bimetallic systems, e.g. sample Pt4Cu1 (13.6 μL h^{-1} cm^{-2}) or Pt1Cu4 (19.5 μL h^{-1} cm^{-2}), is only slightly higher than that of sample Pt5. Nevertheless, it is remarkable that for Cu NPs the incorporation of small amounts of Pt, as in sample Pt1Cu4, leads to activities that are higher than that of sample Pt5, which indeed contains a (nominally) 5 times higher Pt loading.

To evaluate the effects of the overall co-catalyst loading on the H_2 evolution activity, a series of samples was produced by dewetting on NTs bilayers with different nominal thicknesses but a constant Pt:Cu thickness ratio of 1:1. These structures are shown in Fig. S6. The SEM data show that in any case the NTs are homogeneously decorated with bimetallic PtCu NPS. It is clear that the thicker the bilayer, the larger the PtCu NP size which show an average diameter of 5-10, 5-15 and 25-35 nm for samples Pt1Cu1, Pt2.5Cu2.5 and Pt5Cu5, respectively. The photocatalytic performance of these structures is shown in Fig. 5b. The results show that dewetting of bilayers with a nominal thickness of Pt 2.5 nm and Cu 2.5 nm leads to the most effective co-catalytic effects.

After evaluating the effects of the relative Pt:Cu amount, we carried out control experiments by producing a series of TiO_2 NT layers decorated with different loadings of dewetted Pt NPs. For this, the initial Pt loading was systematically screened by sputter-depositing 0.5, 1, 2.5, 5 and 10 nm-thick Pt films followed by dewetting (500°C, Ar, 1h). Fig. 5c shows the photocatalytic H_2 evolution rates of Pt-TiO_2 structures. The data show a typical volcano trend, where the increase of the co-catalyst loading leads initially to an activity enhancement. Sample Pt2.5 is the most active photocatalyst, with a H_2 evolution rate of 25.8 μL h^{-1} cm^{-2}, which is still 50% lower than the activity of the optimized bimetallic co-catalyst (sample Pt2.5Cu2.5) in spite of the virtually identical Pt content. Higher Pt loadings lead to suboptimum photocatalytic efficiencies (as also observed in previous work[8,44,54]) likely due to a larger size of the dewetted NPs and consequently to their lower active surface area.

The higher activities reported in previous studies for Pt and Cu modified photocatalysts were attributed to Cu plasmonic effects[27,55] or Cu^{2+}/Cu^{+} photosensitization mechanisms.[56] To enable the latter effect in Pt-Cu bimetallic systems, the formation of PtCu alloys was purposely avoided,

being reported to be detrimental for the photoactivity.[23] Irie et al., and Dozzi and co-workers in follow up work, proposed that since the redox potential of the Cu^{2+}/Cu^{+} couple (for amorphous Cu(II) oxide decorations) or the CB minima of crystalline CuO are less negative than the CB of TiO_2, Cu^{2+} species on the TiO_2 surface may capture TiO_2 CB electrons causing a consequent one-electron reduction of oxidized copper species (Cu^{2+} to Cu^{+}) meanwhile enhancing the charge carrier separation efficiency.[23,56] This effect, was reported to come along with visible light activation as electrons in the VB of TiO_2 are directly transferred to the discrete energy levels of grafted Cu^{2+} species (hence causing visible light absorption).

For what concerns our work, annealing titania in argon (or in a reducing environment e.g. H_2/Ar) may produce oxygen vacancies in the oxide, as extensively reported in the literature (examples can be found in refs.[57–61]). Structures crystallized by air annealing would provide a suitable reference material to assess the effect of the Ar treatment and the associated formation of oxygen vacancies. Nevertheless, air annealing is not suitable to induce dewetting (and alloying) of Pt, Cu or Pt-Cu films. As found in previous work,[13,44,61,54] such metals are susceptible to oxygen and tend to easily oxide, particularly when exposed to oxygen at high temperatures – their oxidation, in turn, prevents metal atom surface mobility and impair dewetting and NP formation. In other words, air treated structures would differ from samples annealed in argon not only in the density of oxygen vacancies but also in the nature (morphology and composition) of the co-catalyst, this making the direct comparison meaningless.

We should however point out that, for the argon treated samples, possible effects associated to oxygen vacancies formation should be comparable for any samples, since all samples were treated under the same conditions (500°C, pure argon, 1 h). Such effects may be e.g. a higher mobility for

majority carriers (increased conductivity for CB electrons),[58,63] or visible light activation, e.g. due to the introduction of sub CB energy levels causing a narrowing of the oxide optical band gap.[58,59] We assessed the optical properties of pristine NTs and Cu-, Pt-, and PtCu-modified structures by measuring UV-Vis diffuse reflectance spectra. The results are shown Fig. S8. According to the spectra, the band gap (E_g) absorption, for $\lambda \sim \leq 400$ nm, is clear for pristine NTs (black curve). The onset of light absorption is in line with the mixed anatase/rutile composition of the TiO_2 NTs. The absorption band(s) in the visible spectral range, as observed in recent work,[64] can be assigned to interference fringes due to the NT barrier layer (NT bottom) at the substrate/NT interface. The presence of dewetted NPs on the NTs introduces additional complex optical features (likely due to their reflectance). Note that in the presence of the dewetted metal NPs, not only different optical characteristics appear in the visible spectral range, but also becomes the TiO_2 band gap absorption (with predicted onset at λ ca. 400 nm) indistinguishable.

We carried out H_2 evolution experiments with the most active sample (Pt2.5Cu2.5) under irradiation provided by a filtered (420 nm cutoff) AM1.5 simulated solar light and by a monochromatic 450 nm laser (2 W, OdicForce Lasers). Under such experimental conditions, no significant amount of evolved hydrogen could be detected by gas-chromatography. This suggests that the PtCu modified photocatalysts are active under UV light, and hence the improved activity provided by dewetted-alloyed PtCu NPs cannot be ascribed to light absorption features, e.g. to plasmonic effects or to the formation of p-n junctions (in the presence of Cu oxides) or via Cu(II) photo-sensitization effects. Analyzing the UV-Vis spectra (Fig. S8), we noticed in fact that the reflectance of samples 2.5Pt2.5Cu and 5Cu is at 365 nm virtually identical, while the activity of the former is ~ 50 times higher than that of the latter.

Therefore, one can conclude that:

(i) the optical (reflectance) features of the different samples seem not to match the photocatalytic activity trend;

(ii) the oxide charge transport properties cannot be invoked as key factor, as such features are expected to be comparable for all the structures (due to the identical Ar annealing conditions used);

(iii) the key factor affecting the H_2 evolution performance is thus the co-catalyst composition.

The presence of Pt, as clearly shown by XPS and XANES, affects the oxidation state of Cu, which in the bimetallic NPs is present mainly in the metallic form. This may provide Cu in the PtCu system, compared to oxidized Cu species in the pure Cu NPs, with a metal-like co-catalytic ability, i.e. with the ability to trap TiO_2 CB electrons via a metal/semiconductor Schottky junction effect. Pt, on the other hand, is present in the dewetted NPs mainly as metal and its metallic nature remains almost unaltered regardless of the presence or absence of Cu as alloying element. It is also worth to point out that in recent work[65] on Ni-, Cu-, and NiCu-modified TiO_2 we demonstrate that, under illumination, oxidized Ni and Cu species such as native oxides at the co-catalyst surface are promptly reduced to a metallic phase. This can occur either via solid state reduction or through a dissolution/re-deposition process – both mechanisms are triggered by photo-promoted CB electrons. In-situ reduction under photocatalytic conditions was also shown for Pt(IV) species in Pt-TiO_2 systems,[66] and proposed for CuO_x-PtO_2-TiO_2 photocatalysts.[24] Thus, we assume that under the experimental conditions here adopted, oxidized Cu (or Pt) compounds are reduced to their metallic states, which are the active co-catalytic species responsible for the photocatalytic H_2 generation observed. In other words, the different initial Cu speciation in Cu- and PtCu-modified photocatalysts should not be invoked to explain the higher photoactivity of the latter.

Hence, as also proposed by Amal et al.,[24] a most plausible cause for the synergistically enhanced co-catalytic performance is the electronic interaction between Pt and Cu atoms in bimetallic NPs. Such interaction, as supported in their work by XPS results and DFT calculations, is based on the lower electronegativity of Cu with respect to that of Pt. The result is an uneven distribution of the electron density between Pt and Cu that can increase the net electron density on Pt, enhancing the trapping efficiency of photogenerated electrons from the TiO_2 CB. This decreases charge recombination in the semiconductor and consequently improves the photocatalytic H_2 evolution (Scheme S1).[12,24,67] Similar beneficial effects when alloying Pt with Cu were reported also recently for the electrochemical hydrogen evolution reaction (HER).[68]

We assessed the PtCu-TiO_2 photocatalysts also in terms of stability. Fig. 5d shows the amounts of evolved hydrogen vs. the illumination time for sample Pt2.5Cu2.5. Data for sample Pt2.5 are also shown as reference. Sample Pt2.5Cu2.5 under illumination produces H_2 at a constant rate and no initial induction period or deactivation effects at later stages causing loss of activity could be observed. The steady H_2 evolution in the first reaction stage also indicates that the possible in-situ reduction of oxidized Cu species occurs rapidly, i.e. in a timespan of a few minutes, according to what we recently observed by in-situ X-ray absorption spectroscopy.[65] Given the steady H_2 evolution, one may even speculate that reduction of oxidized Cu species occurs in the solid state, i.e. via charge transfer across the PtCu/TiO_2 interface and hence does not involve Cu dissolution/re-deposition mechanisms as reported elsewhere.[65,69]

To validate further the photocatalyst stability, we carried out with the same sample (Pt2.5Cu2.5) a series of repeated photocatalytic cycles. Each photocatalytic run lasted 4 h, and the cycles were repeated for 4 times in a row, after degassing the photocatalytic cell and refreshing the methanol-water mixture. The results (Fig. 5e) show the H_2 evolution activity to be stable and reproducible

for an overall illumination period of 16 h, hence confirming that no photocatalyst deterioration phenomena (NPs detachment or Cu loss) takes place.

Finally, we evaluated the effect of the composition of the methanol-water mixtures on the H_2 evolution activity. Fig. 5f shows the activity of samples Pt2.5Cu2.5 and its monometallic counterpart (Pt2.5) as a function of the methanol content. Such data are also compiled in Fig. 5g in order to show the activity difference ($\Delta_{r_{H_2}}$) between samples Pt2.5Cu2.5 and Pt2.5 for each mixture composition.

According to the results, by increasing the concentration of methanol from 0 vol% to 50 vol% in the reaction solution, the bimetallic catalyst shows a more pronounced increase in photo-activity. When the methanol concentration is further increased to 80%, sample Pt2.5 undergoes an evident deactivation losing 50% of its activity (Fig. 5f). On the contrary, the bimetallic co-catalyst is affected to a minor extent (~15% activity loss) and, as a results, the activity difference ($\Delta_{r_{H_2}}$) between samples Pt2.5Cu2.5 and Pt2.5 monotonically increases when increasing the methanol concentration from 0 to 80 vol% (Fig. 5g). These results may provide an additional explanation for the enhanced activity of bimetallic NPs. One may in fact speculate that PtCu systems provide, compared to Pt NPs, a substantially enhanced tolerance against poisoning from methanol partial oxidation products. Cu atoms in the bimetallic NPs can in fact weaken the binding energy of intermediate adsorbates (such as CO) to surface Pt active sites, as also reported for PtCu catalysts used in methanol fuel cells.[11,70] It is also worth mentioning that previous work on Cu- and PtCu-modified TiO_2 photocatalysts[23] showed that the presence of Cu is key to promote the VB hole mediated oxidation of the hole scavenger to carbon dioxide (complete oxidation) rather than to carbon monoxide (partial oxidation). This was shown to be accompanied by a higher rate of hydrogen production. In other words, the higher selectivity to CO_2 not only may limit the formation

of CO hence preventing CO from blocking H_2 evolution on Pt sites but also can make TiO_2 CB electrons more available for H^+ reduction due to a more efficient VB hole consumption.[71]

4. Conclusions

We used a dewetting-alloying principle to produce, from nm-thick PtCu bilayers, bimetallic PtCu co-catalytic nanoparticles on arrays of TiO_2 nanocavities. We characterized these structures in view of their physicochemical features and photocatalytic H_2 evolution performance. A series of complementary characterization techniques including XRD, XPS and XANES proved the bimetallic nature of the PtCu alloy nanoparticles. TiO_2 nanocavities co-catalyzed by such PtCu nanoalloys can synergistically promote the photocatalytic generation of H_2 from methanol-water mixtures at rates that are substantially higher than those yielded by Pt or Cu monometallic counterparts. The H_2 evolution improvement is ascribed to a Pt-Cu electronic interaction in the co-catalyst NPs that causes a more efficient trapping of TiO_2 CB electrons and transfer to the environment for H_2 evolution.

The results herein discussed contribute another interpretation to the growing debate on the copper oxidation state and role in the photocatalytic hydrogen evolution reaction.

From a more general view point, our work shows that the alloying via solid state dewetting of earth abundant transition metals such as Cu with noble elements (Pt, Pd or Au) can provide intriguing catalytic effects and remarkable activity enhancements along with a more sustainable catalyst economy. Such principle can be adapted to a variety of bimetallic systems of key relevance in photocatalytic or electrochemical conversion processes.

Supporting Information

Additional catalyst characterization data (SEM, particle size statistics, XPS, photocatalytic H_2 evolution activity, UV-Vis, EXAFS) are provided in Figures S1-S8, Scheme S1 and Tables S1-S2.

Acknowledgements

The authors would like to acknowledge the ERC, DFG and the DFG cluster of excellence EAM for financial support. M.A. acknowledges the financial support from the Emerging Talents Initiative ETI (ETI2018/2_Tech_11) provided by the FAU Friedrich Alexander University Erlangen-Nuremberg, Germany. M.A., P.G. and A.M. acknowledge DESY (Hamburg, Germany), a member of the Helmholtz Association HGF, for the provision of experimental facilities. Parts of this research were carried out at DESY – PETRA III (Project I-20190283) and Dr. Edmund Welter is acknowledged for technical assistance in using the photon beamline P65. The research leading to this result has been supported also by the project CALIPSOplus under the Grant Agreement 730872 from the EU Framework Programme for Research and Innovation HORIZON 2020. E.W. acknowledges the Alexander von Humboldt Foundation for providing financial support. A.M. acknowledges "Piano di Sostegno alla Ricerca, Università degli Studi di Milano". P.G. acknowledges financial support by MIUR trough the grant “PRIN 2017, 2017KKP5ZR, MOSCATo”. Helga Hildebrand, Anja Friedrich, Ulrike Marten-Jahns and Alexander Tesler are gratefully acknowledged for technical help.

References

(1) Fujishima, A.; Honda, K. Electrochemical Photolysis of Water at a Semiconductor Electrode. *Nature* **1972**, *238* (5358), 37–38. https://doi.org/10.1038/238037a0.

(2) Roy, P.; Berger, S.; Schmuki, P. TiO2 Nanotubes: Synthesis and Applications. *Angew. Chemie Int. Ed.* **2011**, *50* (13), 2904–2939. https://doi.org/10.1002/anie.201001374.

(3) Spanu, D.; Recchia, S.; Mohajernia, S.; Schmuki, P.; Altomare, M. Site-Selective Pt Dewetting on WO 3 -Coated TiO 2 Nanotube Arrays: An Electron Transfer Cascade-Based H 2 Evolution Photocatalyst. *Appl. Catal. B Environ.* **2018**, *237* (May), 198–205. https://doi.org/10.1016/j.apcatb.2018.05.061.

(4) Chuangchote, S.; Jitputti, J.; Sagawa, T.; Yoshikawa, S. Photocatalytic Activity for Hydrogen Evolution of Electrospun TiO 2 Nanofibers. *ACS Appl. Mater. Interfaces* **2009**, *1* (5), 1140–1143. https://doi.org/10.1021/am9001474.

(5) Linsebigler, A. L.; Lu, G.; Yates, J. T. Photocatalysis on TiOn Surfaces: Principles, Mechanisms, and Selected Results. *Chem. Rev.* **1995**, 735–758. https://doi.org/10.1021/cr00035a013.

(6) Chen, X.; Mao, S. S. Titanium Dioxide Nanomaterials: Synthesis, Properties, Modifications, and Applications. *Chem. Rev.* **2007**, *107* (7), 2891–2959. https://doi.org/10.1021/cr0500535.

(7) Jennings, J. R.; Ghicov, A.; Peter, L. M.; Schmuki, P.; Walker, A. B. Dye-Sensitized Solar Cells Based on Oriented TiO 2 Nanotube Arrays: Transport, Trapping, and Transfer of Electrons. *J. Am. Chem. Soc.* **2008**, *130* (40), 13364–13372. https://doi.org/10.1021/ja804852z.

(8) Nguyen, N. T.; Altomare, M.; Yoo, J.; Schmuki, P. Efficient Photocatalytic H 2 Evolution: Controlled Dewetting-Dealloying to Fabricate Site-Selective High-Activity Nanoporous Au Particles on Highly Ordered TiO 2 Nanotube Arrays. *Adv. Mater.* **2015**, *27* (20), 3208–3215. https://doi.org/10.1002/adma.201500742.

(9) Wang, D.; Liu, Z. P.; Yang, W. M. Proton-Promoted Electron Transfer in Photocatalysis: Key Step for Photocatalytic Hydrogen Evolution on Metal/Titania Composites. *ACS Catal.* **2017**, *7* (4), 2744–2752. https://doi.org/10.1021/acscatal.7b00225.

(10) Chen, T.; Feng, Z.; Wu, G.; Shi, J.; Ma, G.; Ying, P.; Li, C. Mechanistic Studies of Photocatalytic Reaction of Methanol for Hydrogen Production on Pt/TiO 2 by in Situ

Fourier Transform IR and Time-Resolved IR Spectroscopy. *J. Phys. Chem. C* **2007**, *111* (22), 8005–8014. https://doi.org/10.1021/jp071022b.

(11) Liao, Y.; Yu, G.; Zhang, Y.; Guo, T.; Chang, F.; Zhong, C. Composition-Tunable PtCu Alloy Nanowires and Electrocatalytic Synergy for Methanol Oxidation Reaction. *J. Phys. Chem. C* **2016**, *120* (19), 10476–10484. https://doi.org/10.1021/acs.jpcc.6b02630.

(12) Dimitrova, N.; Dhifallah, M.; Mineva, T.; Boiadjieva-Scherzer, T.; Guesmi, H.; Georgieva, J. High Performance of PtCu@TiO 2 Nanocatalysts toward Methanol Oxidation Reaction: From Synthesis to Molecular Picture Insight. *RSC Adv.* **2019**, *9* (4), 2073–2080. https://doi.org/10.1039/C8RA08782B.

(13) Ji, L.; Spanu, D.; Denisov, N.; Recchia, S.; Schmuki, P.; Altomare, M. A Dewetted-dealloyed Nanoporous Pt Co-catalyst Formed on TiO2 Nanotube Arrays Leads to Strongly Enhanced Photocatalytic H2 Production. *Chem. – An Asian J.* **2019**, asia.201901545. https://doi.org/10.1002/asia.201901545.

(14) Kugai, J.; Moriya, T.; Seino, S.; Nakagawa, T.; Ohkubo, Y.; Nitani, H.; Mizukoshi, Y.; Yamamoto, T. A. Effect of Support for PtCu Bimetallic Catalysts Synthesized by Electron Beam Irradiation Method on Preferential CO Oxidation. *Appl. Catal. B Environ.* **2012**, *126*, 306–314. https://doi.org/10.1016/j.apcatb.2012.07.028.

(15) Okuhara, T.; Miura, H. Metallic Catalysts. *Hyomen Kagaku* **1988**, *9* (9), 676–683. https://doi.org/10.1380/jsssj.9.676.

(16) Papadimitriou, S.; Armyanov, S.; Valova, E.; Hubin, A.; Steenhaut, O.; Pavlidou, E.; Kokkinidis, G.; Sotiropoulos, S. Methanol Oxidation at Pt-Cu, Pt-Ni, and Pt-Co Electrode Coatings Prepared by a Galvanic Replacement Process. *J. Phys. Chem. C* **2010**, *114* (11), 5217–5223. https://doi.org/10.1021/jp911568g.

(17) Lyu, L.-M.; Kao, Y.-C.; Cullen, D. A.; Sneed, B. T.; Chuang, Y.-C.; Kuo, C.-H. Spiny Rhombic Dodecahedral CuPt Nanoframes with Enhanced Catalytic Performance Synthesized from Cu Nanocube Templates. *Chem. Mater.* **2017**, *29* (13), 5681–5692. https://doi.org/10.1021/acs.chemmater.7b01550.

(18) Lee, S.; Jeong, S.; Kim, W. D.; Lee, S.; Lee, K.; Bae, W. K.; Moon, J. H.; Lee, S.; Lee, D. C. Low-Coordinated Surface Atoms of CuPt Alloy Cocatalysts on TiO 2 for Enhanced Photocatalytic Conversion of CO 2. *Nanoscale* **2016**, *8* (19), 10043–10048. https://doi.org/10.1039/C6NR02124G.

(19) Zhou, S.; Varughese, B.; Eichhorn, B.; Jackson, G.; McIlwrath, K. Pt-Cu Core-Shell and Alloy Nanoparticles for Heterogeneous NOx Reduction: Anomalous Stability and Reactivity of a Core-Shell Nanostructure. *Angew. Chemie Int. Ed.* **2005**, *44* (29), 4539–4543. https://doi.org/10.1002/anie.200500919.

(20) Xiang, H.; Zheng, Y.; Sun, Y.; Guo, T.; Zhang, P.; Li, W.; Kong, S.; Ouzounian, M.; Chen, H.; Li, H.; Hu, T. S.; Yu, G.; Feng, Y.; Liu, S. Bimetallic and Postsynthetically Alloyed PtCu Nanostructures with Tunable Reactivity for the Methanol Oxidation Reaction. *Nanoscale Adv.* **2020**, *2* (4), 1603–1612. https://doi.org/10.1039/D0NA00076K.

(21) Yang, H.; Dai, L.; Xu, D.; Fang, J.; Zou, S. Electrooxidation of Methanol and Formic Acid on PtCu Nanoparticles. *Electrochim. Acta* **2010**, *55* (27), 8000–8004. https://doi.org/10.1016/j.electacta.2010.03.026.

(22) Khan, I. A.; Qian, Y.; Badshah, A.; Zhao, D.; Nadeem, M. A. Fabrication of Highly Stable and Efficient PtCu Alloy Nanoparticles on Highly Porous Carbon for Direct Methanol Fuel Cells. *ACS Appl. Mater. Interfaces* **2016**, *8* (32), 20793–20801. https://doi.org/10.1021/acsami.6b06068.

(23) Dozzi, M. V.; Chiarello, G. L.; Pedroni, M.; Livraghi, S.; Giamello, E.; Selli, E. High Photocatalytic Hydrogen Production on Cu(II) Pre-Grafted Pt/TiO 2. *Appl. Catal. B Environ.* **2017**, *209* (Ii), 417–428. https://doi.org/10.1016/j.apcatb.2017.03.007.

(24) Jung, M.; Hart, J. N.; Boensch, D.; Scott, J.; Ng, Y. H.; Amal, R. Hydrogen Evolution via Glycerol Photoreforming over Cu–Pt Nanoalloys on TiO2. *Appl. Catal. A Gen.* **2016**, *518*, 221–230. https://doi.org/10.1016/j.apcata.2015.10.040.

(25) Sinatra, L.; LaGrow, A. P.; Peng, W.; Kirmani, A. R.; Amassian, A.; Idriss, H.; Bakr, O. M. A Au/Cu 2 O–TiO 2 System for Photo-Catalytic Hydrogen Production. A Pn-Junction Effect or a Simple Case of in Situ Reduction? *J. Catal.* **2015**, *322*, 109–117. https://doi.org/10.1016/j.jcat.2014.11.012.

(26) Kar, P.; Zhang, Y.; Mahdi, N.; Thakur, U. K.; Wiltshire, B. D.; Kisslinger, R.; Shankar, K. Heterojunctions of Mixed Phase TiO 2 Nanotubes with Cu, CuPt, and Pt Nanoparticles: Interfacial Band Alignment and Visible Light Photoelectrochemical Activity. *Nanotechnology* **2018**, *29* (1), 14002. https://doi.org/10.1088/1361-6528/aa9823.

(27) Shiraishi, Y.; Sakamoto, H.; Sugano, Y.; Ichikawa, S.; Hirai, T. Pt-Cu Bimetallic Alloy Nanoparticles Supported on Anatase TiO2: Highly Active Catalysts for Aerobic Oxidation

Driven by Visible Light. *ACS Nano* **2013**, *7* (10), 9287–9297. https://doi.org/10.1021/nn403954p.

(28) Srabionyan, V. V.; Pryadchenko, V. V.; Kurzin, A. A.; Belenov, S. V.; Avakyan, L. A.; Guterman, V. E.; Bugaev, L. A. Atomic Structure of PtCu Nanoparticles in PtCu/C Catalysts from EXAFS Spectroscopy Data. *Phys. Solid State* **2016**, *58* (4), 752–762. https://doi.org/10.1134/S1063783416040247.

(29) Toshima, N.; Wang, Y. Preparation and Catalysis of Novel Colloidal Dispersions of Copper/Noble Metal Bimetallic Clusters. *Langmuir* **1994**, *10* (12), 4574–4580. https://doi.org/10.1021/la00024a031.

(30) Spanu, D.; Recchia, S.; Mohajernia, S.; Tomanec, O.; Kment, Š.; Zboril, R.; Schmuki, P.; Altomare, M. Templated Dewetting–Alloying of NiCu Bilayers on TiO 2 Nanotubes Enables Efficient Noble-Metal-Free Photocatalytic H 2 Evolution. *ACS Catal.* **2018**, *8* (6), 5298–5305. https://doi.org/10.1021/acscatal.8b01190.

(31) Thompson, C. V. Solid-State Dewetting of Thin Films. *Annu. Rev. Mater. Res.* **2012**, *42* (1), 399–434. https://doi.org/10.1146/annurev-matsci-070511-155048.

(32) Ono, S.; Saito, M.; Asoh, H. Self-Ordering of Anodic Porous Alumina Formed in Organic Acid Electrolytes. *Electrochim. Acta* **2005**, *51* (5), 827–833. https://doi.org/10.1016/j.electacta.2005.05.058.

(33) Houser, J. E.; Hebert, K. R. The Role of Viscous Flow of Oxide in the Growth of Self-Ordered Porous Anodic Alumina Films. *Nat. Mater.* **2009**, *8* (5), 415–420. https://doi.org/10.1038/nmat2423.

(34) Hebert, K. R.; Albu, S. P.; Paramasivam, I.; Schmuki, P. Morphological Instability Leading to Formation of Porous Anodic Oxide Films. *Nat. Mater.* **2012**, *11* (2), 162–166. https://doi.org/10.1038/nmat3185.

(35) Yoo, J. E.; Schmuki, P. Critical Factors in the Anodic Formation of Extremely Ordered Titania Nanocavities. *J. Electrochem. Soc.* **2019**, *166* (11), C3389–C3398. https://doi.org/10.1149/2.0381911jes.

(36) Altomare, M.; Nguyen, N. T.; Schmuki, P. Templated Dewetting: Designing Entirely Self-Organized Platforms for Photocatalysis. *Chem. Sci.* **2016**, *7* (12), 6865–6886. https://doi.org/10.1039/C6SC02555B.

(37) Ravel, B.; Newville, M. ATHENA and ARTEMIS Interactive Graphical Data

Analysisusing IFEFFIT. *Phys. Scr.* **2005**, *T115*, 1007. https://doi.org/10.1238/Physica.Topical.115a01007.

(38) Yoo, J. E.; Lee, K.; Altomare, M.; Selli, E.; Schmuki, P. Self-Organized Arrays of Single-Metal Catalyst Particles in TiO 2 Cavities: A Highly Efficient Photocatalytic System. *Angew. Chemie Int. Ed.* **2013**, *52* (29), 7514–7517. https://doi.org/10.1002/anie.201302525.

(39) El-Deeb, H.; Bron, M. Microwave-Assisted Polyol Synthesis of PtCu/carbon Nanotube Catalysts for Electrocatalytic Oxygen Reduction. *J. Power Sources* **2015**, *275*, 893–900. https://doi.org/10.1016/j.jpowsour.2014.11.060.

(40) Herz, A.; Wang, D.; Müller, R.; Schaaf, P. Formation of Supersaturated Au-Ni Nanoparticles via Dewetting of an Au/Ni Bilayer. *Mater. Lett.* **2013**, *102–103*, 22–25. https://doi.org/10.1016/j.matlet.2013.03.096.

(41) Denton, A. R.; Ashcroft, N. W. Vegard's Law. *Phys. Rev. A* **1991**, *43* (6), 3161–3164. https://doi.org/10.1103/PhysRevA.43.3161.

(42) Liu, Y.; Huang, Y.; Xie, Y.; Yang, Z.; Huang, H.; Zhou, Q. Preparation of Highly Dispersed CuPt Nanoparticles on Ionic-Liquid-Assisted Graphene Sheets for Direct Methanol Fuel Cell. *Chem. Eng. J.* **2012**, *197*, 80–87. https://doi.org/10.1016/j.cej.2012.05.011.

(43) Liu, J.; Liu, M.; Yang, X.; Chen, H.; Liu, S. F.; Yan, J. Photo-Redeposition Synthesis of Bimetal Pt–Cu Co-Catalysts for TiO 2 Photocatalytic Solar-Fuel Production. *ACS Sustain. Chem. Eng.* **2020**, *8* (15), 6055–6064. https://doi.org/10.1021/acssuschemeng.0c00969.

(44) Yoo, J.; Altomare, M.; Mokhtar, M.; Alshehri, A.; Al-Thabaiti, S. A.; Mazare, A.; Schmuki, P. Photocatalytic H 2 Generation Using Dewetted Pt-Decorated TiO 2 Nanotubes: Optimized Dewetting and Oxide Crystallization by a Multiple Annealing Process. *J. Phys. Chem. C* **2016**, *120* (29), 15884–15892. https://doi.org/10.1021/acs.jpcc.5b12050.

(45) Mohajernia, S.; Hejazi, S.; Andryskova, P.; Zoppellaro, G.; Tomanec, O.; Zboril, R.; Schmuki, P. Conductive Cu-Doped TiO 2 Nanotubes for Enhanced Photoelectrochemical Methanol Oxidation and Concomitant Hydrogen Generation. *ChemElectroChem* **2019**, *6* (4), 1244–1249. https://doi.org/10.1002/celc.201900076.

(46) Myles, K. .; Darby, J. . Thermodynamic Properties of Solid Palladuim-Copper and

Platinum-Copper Alloys. *Acta Metall.* **1968**, *16* (4), 485–492. https://doi.org/10.1016/0001-6160(68)90122-3.

(47) Wakisaka, M.; Mitsui, S.; Hirose, Y.; Kawashima, K.; Uchida, H.; Watanabe, M. Electronic Structures of Pt-Co and Pt-Ru Alloys for CO-Tolerant Anode Catalysts in Polymer Electrolyte Fuel Cells Studied by EC-XPS. *J. Phys. Chem. B* **2006**, *110* (46), 23489–23496. https://doi.org/10.1021/jp0653510.

(48) Liu, J.; Liu, M.; Yang, X.; Chen, H.; Liu, S. F.; Yan, J. Photo-Redeposition Synthesis of Bimetal Pt–Cu Co-Catalysts for TiO 2 Photocatalytic Solar-Fuel Production. *ACS Sustain. Chem. Eng.* **2020**, *8* (15), 6055–6064. https://doi.org/10.1021/acssuschemeng.0c00969.

(49) Bahruji, H.; Bowker, M.; Davies, P. R.; Pedrono, F. New Insights into the Mechanism of Photocatalytic Reforming on Pd/TiO2. *Appl. Catal. B Environ.* **2011**, *107* (1–2), 205–209. https://doi.org/10.1016/j.apcatb.2011.07.015.

(50) Lytle, F. W.; Wei, P. S. P.; Greegor, R. B.; Via, G. H.; Sinfelt, J. H. Effect of Chemical Environment on Magnitude of X-ray Absorption Resonance at L I I I Edges. Studies on Metallic Elements, Compounds, and Catalysts. *J. Chem. Phys.* **1979**, *70* (11), 4849–4855. https://doi.org/10.1063/1.437376.

(51) Bamwenda, G. R.; Tsubota, S.; Kobayashi, T.; Haruta, M. Photoinduced Hydrogen Production from an Aqueous Solution of Ethylene Glycol over Ultrafine Gold Supported on TiO2. *J. Photochem. Photobiol. A Chem.* **1994**, *77* (1), 59–67. https://doi.org/10.1016/1010-6030(94)80009-X.

(52) Bamwenda, G. R.; Tsubota, S.; Nakamura, T.; Haruta, M. <(J.Photochem.Photobiol.A-Chem)[1995]Photoassisted Hydrogen Production from a Water-Ethanol Solution-a Comparison of Activities of Au@TiO2 and Pr@TiO2.pdf>. **1995**, *89*, 177–189.

(53) Naldoni, A.; D'Arienzo, M.; Altomare, M.; Marelli, M.; Scotti, R.; Morazzoni, F.; Selli, E.; Dal Santo, V. Pt and Au/TiO2 Photocatalysts for Methanol Reforming: Role of Metal Nanoparticles in Tuning Charge Trapping Properties and Photoefficiency. *Appl. Catal. B Environ.* **2013**, *130–131*, 239–248. https://doi.org/10.1016/j.apcatb.2012.11.006.

(54) Nguyen, N. T.; Yoo, J.; Altomare, M.; Schmuki, P. "Suspended" Pt Nanoparticles over TiO 2 Nanotubes for Enhanced Photocatalytic H 2 Evolution. *Chem. Commun.* **2014**, *50* (68), 9653–9656. https://doi.org/10.1039/C4CC04087B.

(55) Zhang, L.; Jia, C.; He, S.; Zhu, Y.; Wang, Y.; Zhao, Z.; Gao, X.; Zhang, X.; Sang, Y.;

Zhang, D.; Xu, X.; Liu, H. Hot Hole Enhanced Synergistic Catalytic Oxidation on Pt-Cu Alloy Clusters. *Adv. Sci.* **2017**, *4* (6). https://doi.org/10.1002/advs.201600448.

(56) Irie, H.; Kamiya, K.; Shibanuma, T.; Miura, S.; Tryk, D. A.; Yokoyama, T.; Hashimoto, K. Visible Light-Sensitive Cu(II)-Grafted TiO2 Photocatalysts: Activities and X-Ray Absorption Fine Structure Analyses. *J. Phys. Chem. C* **2009**, *113* (24), 10761–10766. https://doi.org/10.1021/jp903063z.

(57) Mohajernia, S.; Hejazi, S.; Mazare, A.; Nguyen, N. T.; Schmuki, P. Photoelectrochemical H 2 Generation from Suboxide TiO 2 Nanotubes: Visible-Light Absorption versus Conductivity. *Chem. - A Eur. J.* **2017**, *23* (50), 12406–12411. https://doi.org/10.1002/chem.201702245.

(58) Naldoni, A.; Altomare, M.; Zoppellaro, G.; Liu, N.; Kment, Š.; Zbořil, R.; Schmuki, P. Photocatalysis with Reduced TiO 2 : From Black TiO 2 to Cocatalyst-Free Hydrogen Production. *ACS Catal.* **2019**, *9* (1), 345–364. https://doi.org/10.1021/acscatal.8b04068.

(59) Mohajernia, S.; Andryskova, P.; Zoppellaro, G.; Hejazi, S.; Kment, S.; Zboril, R.; Schmidt, J.; Schmuki, P. Influence of Ti 3+ Defect-Type on Heterogeneous Photocatalytic H 2 Evolution Activity of TiO 2. *J. Mater. Chem. A* **2020**, *8* (3), 1432–1442. https://doi.org/10.1039/C9TA10855F.

(60) Liu, N.; Häublein, V.; Zhou, X.; Venkatesan, U.; Hartmann, M.; Mačković, M.; Nakajima, T.; Spiecker, E.; Osvet, A.; Frey, L.; Schmuki, P. "Black" TiO 2 Nanotubes Formed by High-Energy Proton Implantation Show Noble-Metal- Co -Catalyst Free Photocatalytic H 2 -Evolution. *Nano Lett.* **2015**, *15* (10), 6815–6820. https://doi.org/10.1021/acs.nanolett.5b02663.

(61) Naldoni, A.; Fabbri, F.; Altomare, M.; Marelli, M.; Psaro, R.; Selli, E.; Salviati, G.; Dal Santo, V. The Critical Role of Intragap States in the Energy Transfer from Gold Nanoparticles to TiO 2. *Phys. Chem. Chem. Phys.* **2015**, *17* (7), 4864–4869. https://doi.org/10.1039/C4CP05775A.

(62) Nguyen, N. T.; Altomare, M.; Yoo, J. E.; Taccardi, N.; Schmuki, P. Noble Metals on Anodic TiO 2 Nanotube Mouths: Thermal Dewetting of Minimal Pt Co-Catalyst Loading Leads to Significantly Enhanced Photocatalytic H 2 Generation. *Adv. Energy Mater.* **2016**, *6* (2), 1501926. https://doi.org/10.1002/aenm.201501926.

(63) Mohajernia, S.; Hejazi, S.; Mazare, A.; Nguyen, N. T.; Hwang, I.; Kment, S.; Zoppellaro,

G.; Tomanec, O.; Zboril, R.; Schmuki, P. Semimetallic Core-Shell TiO 2 Nanotubes as a High Conductivity Scaffold and Use in Efficient 3D-RuO 2 Supercapacitors. *Mater. Today Energy* **2017**, *6*, 46–52. https://doi.org/10.1016/j.mtener.2017.08.001.

(64) Tesler, A. B.; Altomare, M.; Schmuki, P.; Accepted, J. Morphology and Optical Properties of Highly Ordered TiO 2 Nanotubes Grown in NH 4 F / O-H 3 PO 4 Electrolytes in View of Light Harvesting and Catalytic Applications. **2020**. https://doi.org/10.1021/acsanm.0c01859.

(65) Spanu, D.; Minguzzi, A.; Recchia, S.; Shahvardanfard, F.; Tomanec, O.; Zbořil, R.; Schmuki, P.; Ghigna, P.; Altomare, M. An Operando X-Ray Absorption Spectroscopy Study of a NiCu-TiO2 Photocatalyst for H2 Evolution. *ACS Catal.* **2020**, acscatal.0c01373. https://doi.org/10.1021/acscatal.0c01373.

(66) Chiarello, G. L.; Dozzi, M. V.; Scavini, M.; Grunwaldt, J. D.; Selli, E. One Step Flame-Made Fluorinated Pt/TiO2 Photocatalysts for Hydrogen Production. *Appl. Catal. B Environ.* **2014**, *160–161* (1), 144–151. https://doi.org/10.1016/j.apcatb.2014.05.006.

(67) Venkateswara Rao, C.; Viswanathan, B. ORR Activity and Direct Ethanol Fuel Cell Performance of Carbon-Supported Pt−M (M = Fe, Co, and Cr) Alloys Prepared by Polyol Reduction Method. *J. Phys. Chem. C* **2009**, *113* (43), 18907–18913. https://doi.org/10.1021/jp9041606.

(68) Du, Y.; Ni, K.; Zhai, Q.; Yun, Y.; Xu, Y.; Sheng, H.; Zhu, Y.; Zhu, M. Facile Air Oxidative Induced Dealloying of Hierarchical Branched PtCu Nanodendrites with Enhanced Activity for Hydrogen Evolution. *Appl. Catal. A Gen.* **2018**, *557* (January), 72–78. https://doi.org/10.1016/j.apcata.2018.03.014.

(69) Hejazi, S.; Mohajernia, S.; Wu, Y.; Andryskova, P.; Zoppellaro, G.; Hwang, I.; Tomanec, O.; Zboril, R.; Schmuki, P. Intrinsic Cu Nanoparticle Decoration of TiO2 Nanotubes: A Platform for Efficient Noble Metal Free Photocatalytic H2 Production. *Electrochem. commun.* **2019**, *98* (November 2018), 82–86. https://doi.org/10.1016/j.elecom.2018.11.020.

(70) Lu, L.; Chen, S.; Thota, S.; Wang, X.; Wang, Y.; Zou, S.; Fan, J.; Zhao, J. Composition Controllable Synthesis of PtCu Nanodendrites with Efficient Electrocatalytic Activity for Methanol Oxidation Induced by High Index Surface and Electronic Interaction. *J. Phys. Chem. C* **2017**, *121* (36), 19796–19806. https://doi.org/10.1021/acs.jpcc.7b05629.

(71) Chiarello, G. L.; Aguirre, M. H.; Selli, E. Hydrogen Production by Photocatalytic Steam Reforming of Methanol on Noble Metal-Modified TiO2. *J. Catal.* **2010**, *273* (2), 182–190. https://doi.org/10.1016/j.jcat.2010.05.012.

Figure captions

Figure 1 SEM images of different TiO_2 nanotube arrays: (a) pristine NTs (inset shows a cross-sectional view); (b-f) NTs decorated with NPs dewetted from (b) 5 nm-thick Pt film; (c) PtCu bilayer with 4 nm Pt – 1 nm Cu); (d) PtCu bilayer with 2.5 nm Pt − 2.5 nm Cu (inset shows a cross-sectional view); (e) PtCu bilayer with 1 nm Pt − 4 nm Cu; (f) 5-nm-thick Cu films.

Figure 2 (a) X-ray diffraction (XRD) patterns of TiO_2 nanotube decorated with dewetted Pt, Cu or alloyed PtCu NPs of different compositions; (b) enlarged view of the XRD patterns in (a) in the 44-52° 2θ range.

Figure 3 XPS spectra for (a) Pt 4f region of samples Pt2.5 and Pt2.5Cu2.5, (b) Cu 2p region of samples Cu2.5 and Pt2.5Cu2.5, (c) Pt and Cu speciation determined by fitting the spectra in (a,b).

Figure 4 XAS results at the Pt L_{III}- and Cu K-edges. (a) and (b): XANES spectra at the L_{III}- and Cu K-edges, respectively. The spectra were shifted along the *y* axis for comparison. (c) and (d): Pt L_{III}-edge EXAFS spectra for samples Pt2.5Cu2.5 and Pt5, respectively. Blue and magenta lines: experimental; dark yellow lines: fit according to the model described in the text. (e) and (f): Fourier Transforms of the EXAFS spectra of (c) and (d), respectively.

Figure 5 (a) photocatalytic H_2 evolution rate under UV light illumination measured for different Pt:Cu ratios; (b) photocatalytic H_2 evolution rate under UV light illumination measured for samples dewetted from films of different nominal thicknesses but constant Pt:Cu ratio of 1:1; (c)

photocatalytic H_2 evolution rate under UV light illumination measured for samples dewetted from films of different nominal thicknesses of Pt; (d) evolved H_2 amount over time for samples Pt2.5Cu2.5-TiO_2 and Pt2.5-TiO_2 under UV light illumination; (e) stability test for sample Pt2.5Cu2.5-TiO_2; (f) Photocatalytic H_2 evolution rate for samples Pt-TiO_2 and PtCu-TiO_2 measured in methanol-water mixtures of different compositions under UV light illumination; (g) difference in H_2 evolution rate ($\Delta_{r_{H_2}}$) between samples Pt-TiO_2 and PtCu-TiO_2 plotted as a function of the methanol-water mixture composition.

Figure 1

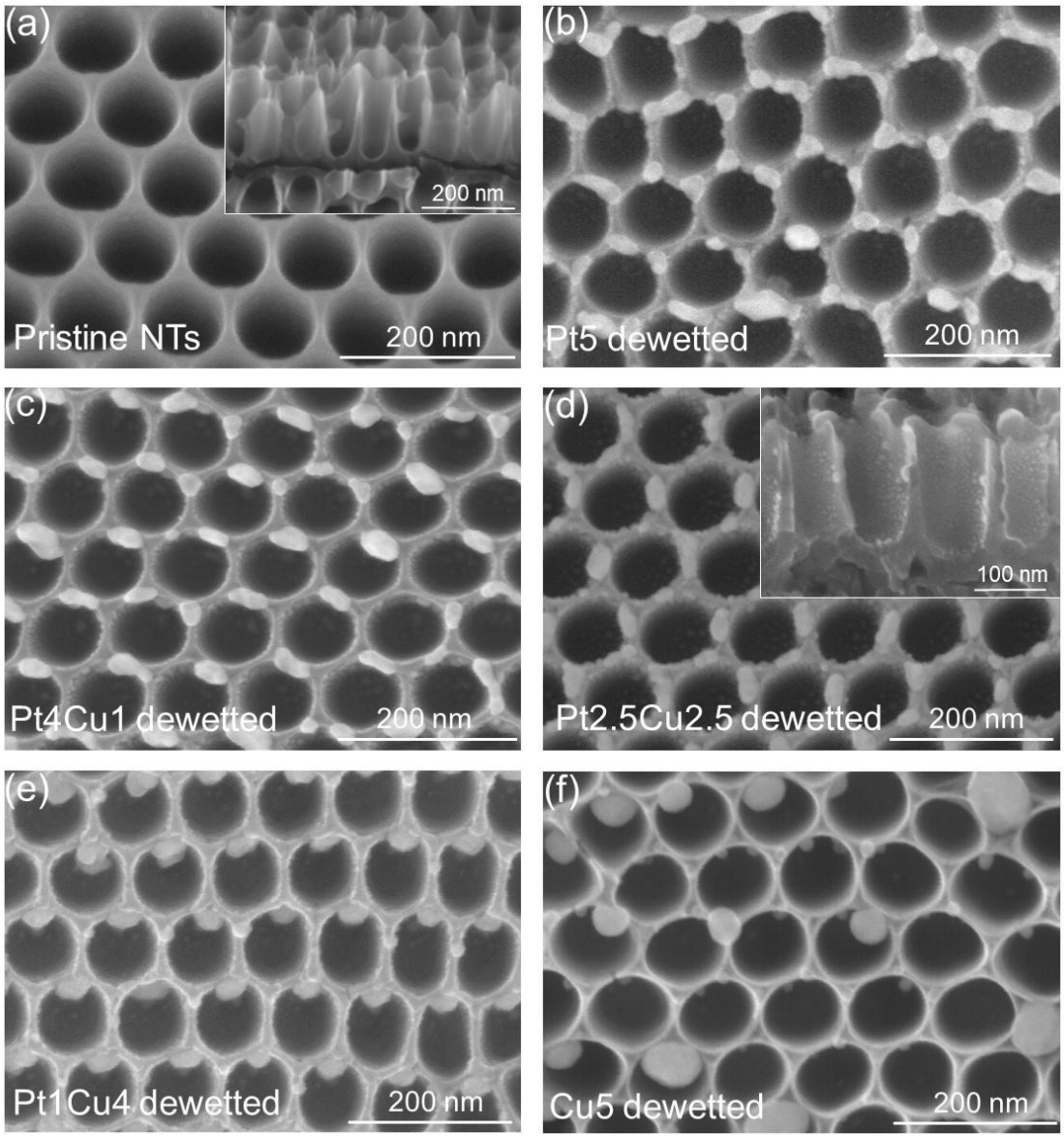
(a)
200 nm
Pristine NTs
200 nm
(b)
Pt5 dewetted
200 nm
(c)
Pt4Cu1 dewetted
200 nm
(d)
100 nm
Pt2.5Cu2.5 dewetted
200 nm
(e)
Pt1Cu4 dewetted
200 nm
(f)
Cu5 dewetted
200 nm

Figure 2

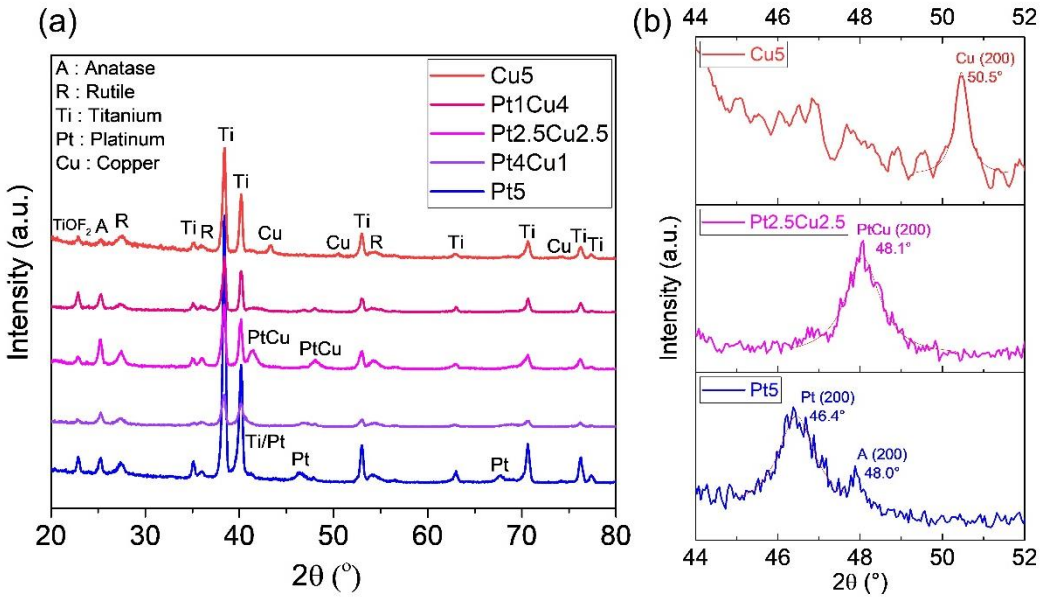
(a)
A : Anatase
R : Rutile
Ti : Titanium
Pt : Platinum
Cu : Copper
Cu5
Pt1Cu4
Pt2.5Cu2.5
Pt4Cu1
Pt5
Intensity (a.u.)
2θ (°)
(b)
Cu5
Cu (200)
50.5°
Pt2.5Cu2.5
PtCu (200)
48.1°
Pt5
Pt (200)
46.4°
A (200)
48.0°

Figure 3

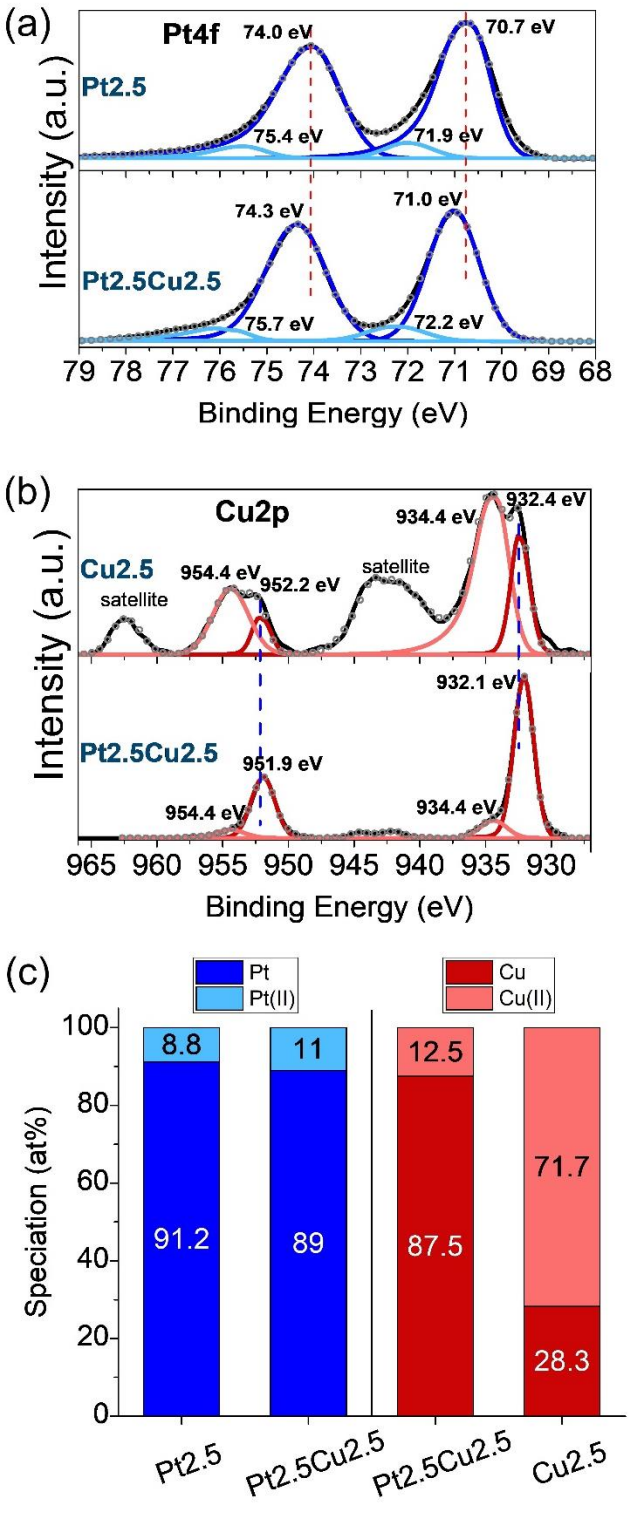
(a)
Pt4f
74.0 eV
70.7 eV
Pt2.5
75.4 eV
71.9 eV
74.3 eV
71.0 eV
Pt2.5Cu2.5
75.7 eV
72.2 eV
Intensity (a.u.)
79 78 77 76 75 74 73 72 71 70 69 68
Binding Energy (eV)
(b)
Cu2p
934.4 eV
932.4 eV
Cu2.5
954.4 eV
952.2 eV
satellite
satellite
932.1 eV
Pt2.5Cu2.5
951.9 eV
954.4 eV
934.4 eV
Intensity (a.u.)
965 960 955 950 945 940 935 930
Binding Energy (eV)
(c)
Pt
Pt(II)
Cu
Cu(II)
Speciation (at%)
100
80
60
40
20
0
8.8
91.2
11
89
12.5
87.5
71.7
28.3
Pt2.5
Pt2.5Cu2.5
Pt2.5Cu2.5
Cu2.5

Figure 4

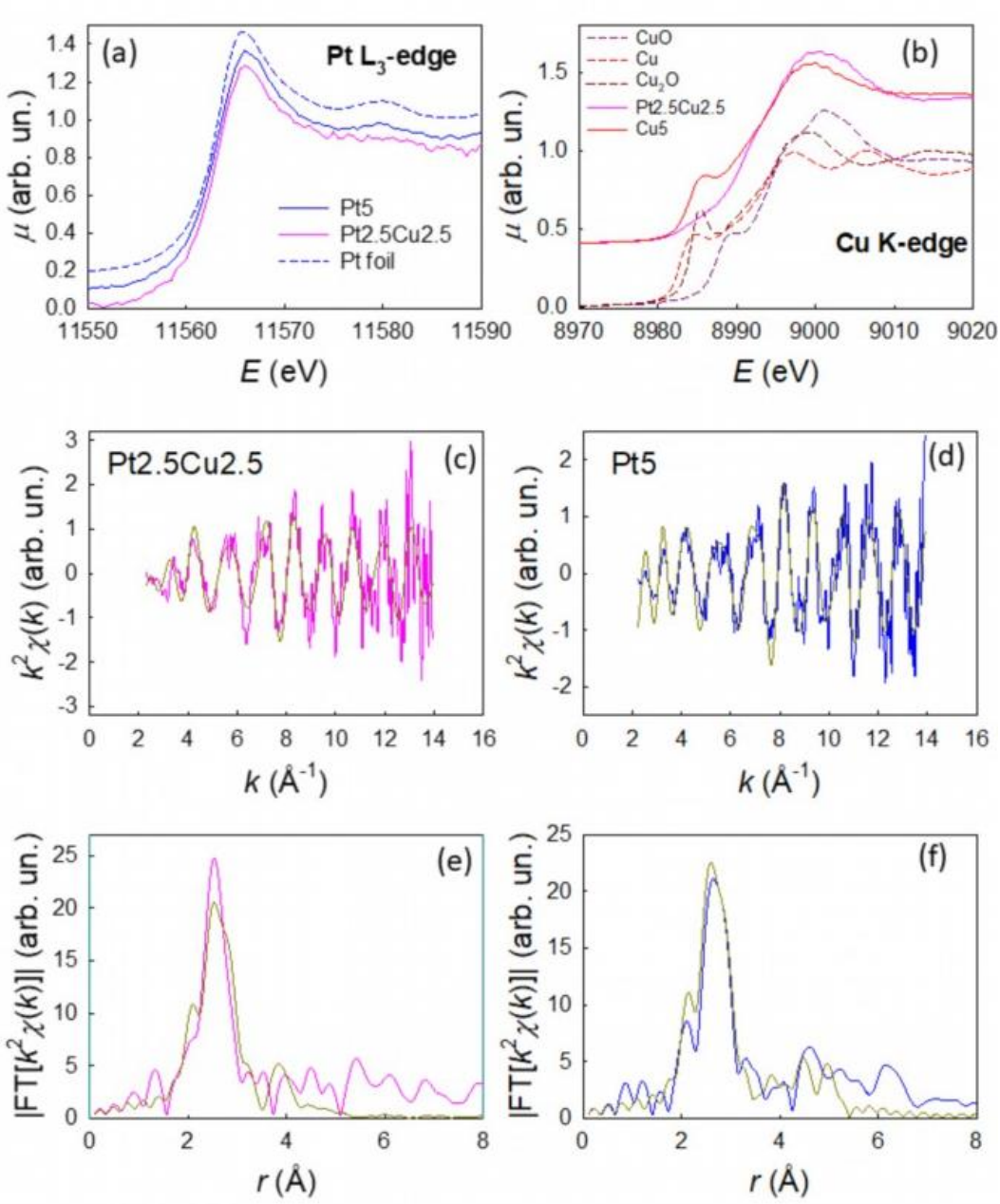
(a)
Pt L3-edge
Pt5
Pt2.5Cu2.5
Pt foil
μ (arb. un.)
E (eV)
(b)
CuO
Cu
Cu2O
Pt2.5Cu2.5
Cu5
Cu K-edge
μ (arb. un.)
E (eV)
Pt2.5Cu2.5
(c)
k2χ(k) (arb. un.)
k (Å-1)
Pt5
(d)
k2χ(k) (arb. un.)
k (Å-1)
(e)
|FT[k2χ(k)]| (arb. un.)
r (Å)
(f)
|FT[k2χ(k)]| (arb. un.)
r (Å)

Figure 5

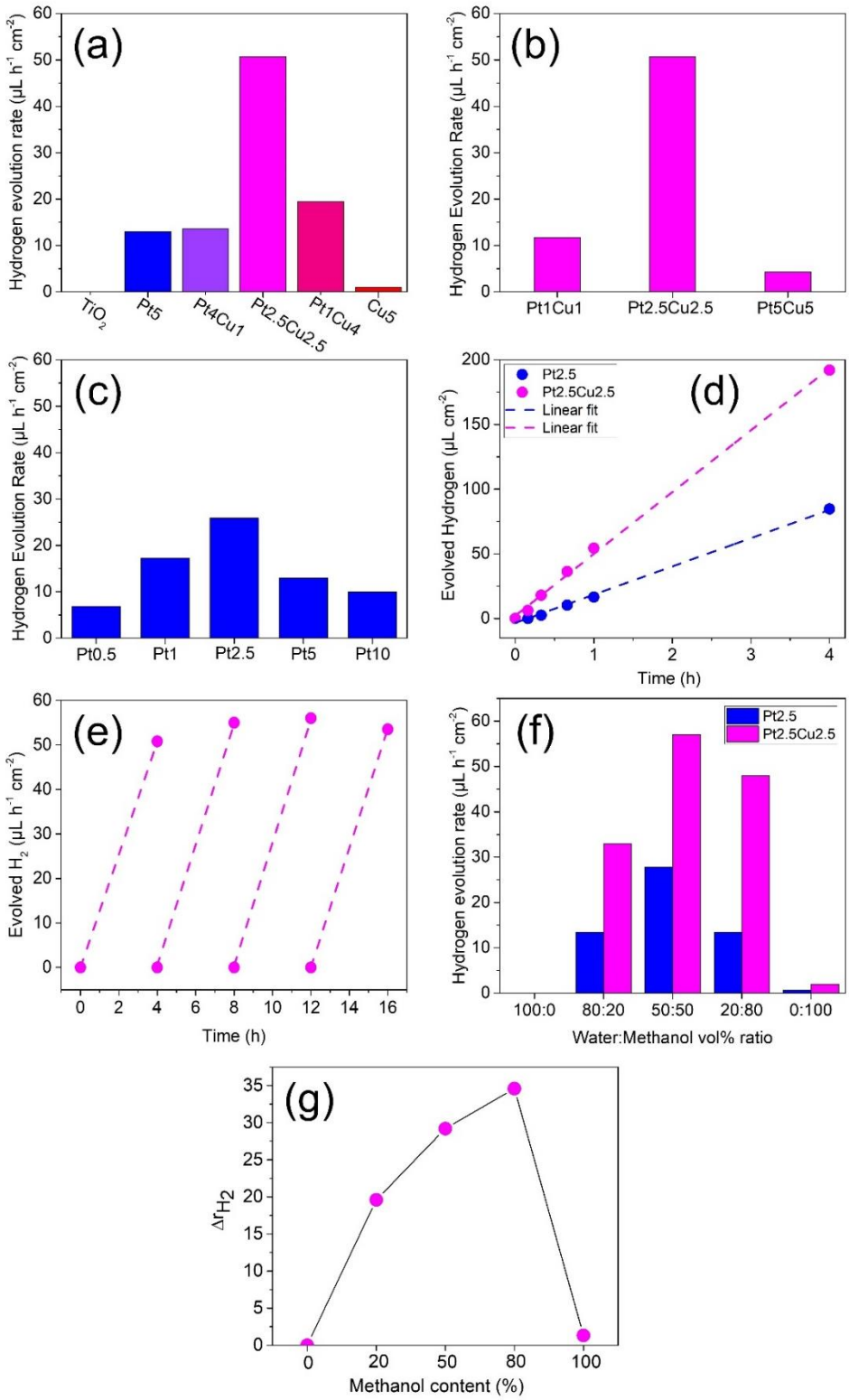
(a)
Hydrogen evolution rate (μL h-1 cm-2)
TiO2
Pt5
Pt4Cu1
Pt2.5Cu2.5
Pt1Cu4
Cu5
(b)
Hydrogen Evolution Rate (μL h-1 cm-2)
Pt1Cu1
Pt2.5Cu2.5
Pt5Cu5
(c)
Hydrogen Evolution Rate (μL h-1 cm-2)
Pt0.5
Pt1
Pt2.5
Pt5
Pt10
(d)
Pt2.5
Pt2.5Cu2.5
Linear fit
Linear fit
Evolved Hydrogen (μL cm-2)
Time (h)
(e)
Evolved H2 (μL h-1 cm-2)
Time (h)
(f)
Pt2.5
Pt2.5Cu2.5
Hydrogen evolution rate (μL h-1 cm-2)
100:0
80:20
50:50
20:80
0:100
Water:Methanol vol% ratio
(g)
ΔrH2
Methanol content (%)

Abstract Graphics